# A Unified MIMO Architecture Subsuming Space Shift Keying, OSTBC, BLAST and LDC

Shinya Sugiura, Sheng Chen and Lajos Hanzo

School of ECS, University of Southampton, SO17 1BJ, UK, Tel: +44-23-8059-3125, Fax: +44-23-8059-4508

Email: {ss07r,sqc,lh}@ecs.soton.ac.uk, http://www-mobile.ecs.soton.ac.uk

*Abstract*—In this paper, motivated by the recent concept of Spatial Modulation (SM), we propose a novel Generalized Space-Time Shift Keying (G-STSK) architecture, which acts as a unified Multiple-Input Multiple-Output (MIMO) framework. More specifically, our G-STSK scheme is based on the rationale that $P$ out of $Q$ dispersion matrices are selected and linearly combined in conjunction with the classic PSK/QAM modulation, where activating $P$ out of $Q$ dispersion matrices provides an implicit means of conveying information bits in addition to the classic modem. Due to its substantial flexibility, our G-STSK framework includes diverse MIMO arrangements, such as SM, Space-Shift Keying (SSK), Linear Dispersion Codes (LDCs), Space-Time Block Codes (STBCs) and Bell Lab's Layered Space-Time (BLAST) scheme. Hence it has the potential of subsuming all of them, when flexibly adapting a set of system parameters. Moreover, we also derive the Discrete-input Continueous-output Memoryless Channel (DCMC) capacity for our G-STSK scheme, which serves as the unified capacity limit, hence quantifying the capacity of diverse MIMO arrangements. Furthermore, EXtrinsic Information Transfer (EXIT) chart analysis is used for designing our G-STSK scheme and for characterizing its iterative decoding convergence.

## I. INTRODUCTION

Over the last two decades diverse Multiple-Input Multiple-Output (MIMO) arrangements have been developed for achieving diversity, multiplexing and/or beamforming gains [1]. For example, while Bell Lab's Layered Space-Time (BLAST) scheme [2] was designed for high-rate transmission, the class of Space-Time Block Codes (STBCs) [3] was developed for achieving a beneficial diversity gain. Furthermore, in [4] Hassibi and Hochwald proposed the unified space-time concept of Linear Dispersion Codes (LDCs), which strikes a flexible tradeoff between the attainable diversity and multiplexing gains.

Recently, Melash *et al.* proposed the sophisticated concept of Spatial Modulation (SM) [5], which employs a novel MIMO encoding principle, where the transmitter activates one out of $M$ transmit Antenna Elements (AEs), whose antenna-activation process acts as an additional means of conveying information bits, and then only the activated antenna transmits a signal modulated with the aid of the classic $\mathcal{L}$-point constellation, such as Phase-Shift Keying (PSK) and Quadrature Amplitude Modulation (QAM). Unlike BLAST, the SM does not transmit simultaneously via $M$ AEs, hence single-antenna-based low-complexity ML detection can be employed at the receiver, while dispensing with symbol-level Inter-Antenna Synchronization (IAS) at the transmitter. The special case of SM is constituted by the scenario, where we deactivate the classic PSK/QAM signalling and simply use the presence or absence of energy assigned to a specific antenna, which is also referred to as Space Shift Keying (SSK) [6]. The SSK was investigated both for uncoded and for turbo-coded scenarios, while the optimal ML detector designed for the uncoded SM/SSK scheme was presented in [7]. Although SM/SSK has the potential of outperforming other MIMO arrangements [5]–[7], SM/SSK was not designed for achieving any transmit diversity gain and hence has to rely on the provision of receive diversity in order to combat the effects of fading channels.

*Against this background, the main contribution of this paper is that we propose a Generalized Space-Time Shift Keying (G-STSK) scheme, where the SM/SSK concept is extended to include two dimensions, namely space as well as time, and hence it becomes capable of striking a flexible tradeoff between the attainable diversity and multiplexing gains. More specifically, in G-STSK $P$ out of $Q$ dispersion matrices are activated during each transmission interval. Owing to its high flexibility, the G-STSK framework subsumes most of the above-mentioned MIMO arrangements, such as SM/SSK, LDC, STBC as well as BLAST, and therefore has the potential of flexibly mimicking all of them. Additionally, we conceive the optimal ML detector designed for uncoded G-STSK systems and the soft-demodulator conceived for the coded G-STSK systems. Moreover, we also derive the Discrete-input Continuous-output Memoryless Channel (DCMC) capacity [8] of our G-STSK scheme, which serves as the unified capacity, hence characterizing diverse MIMO arrangements. EXtrinsic Information Transfer (EXIT) chart analysis [9] is invoked for designing our G-STSK scheme and for characterizing its iterative detection process.*

The remainder of this paper is organized as follows. Section II introduces the system model of our G-STSK scheme, and then both the corresponding hard- and soft-decision detectors are presented in Section III. In Section IV we derive the DCMC capacity of our G-STSK scheme, while Section V provides our performance results. Finally, the paper is concluded in Section VI.

## II. SYSTEM MODEL

In this section we introduce our G-STSK scheme and then demonstrate that it subsumes many MIMO schemes as its special cases.

Let us first consider the general block-based space-time system model of [1]

$$\boldsymbol{Y}(i) = \boldsymbol{H}(i)\boldsymbol{S}(i) + \boldsymbol{V}(i), \tag{1}$$

where $\boldsymbol{Y}(i) \in \mathcal{C}^{N \times T}$ are the signals received at the receiver equipped with $N$ AEs, while $\boldsymbol{S}(i) \in \mathcal{C}^{M \times T}$ represents the space-time codewords transmitted over $T$ symbol durations from the transmitter having $M$ AEs. Furthermore, transmission $i$ represents the block index. It is also assumed that each component of the channel matrix $\boldsymbol{H}(i) \in \mathcal{C}^{N \times M}$ and the noise matrix $\boldsymbol{V}(i) \in \mathcal{C}^{N \times T}$ obeys the complex-valued Gaussian distribution of $\mathcal{CN}(0, 1)$ and $\mathcal{CN}(0, N_0)$, respectively, where $N_0$ represents the noise variance.

### A. G-STSK Modulation

Fig. 1 shows the schematic of our G-STSK's transmitter. In the G-STSK bit-to-symbol mapping scheme, $B = \log_2 f(Q, P) + P \log_2 \mathcal{L}$ bits per block are mapped to a space-time codeword $\boldsymbol{S}(i)$, where $f(Q, P)$ is calculated from $Q$ and $P$ as $f(Q, P) = 2^\iota$, while the
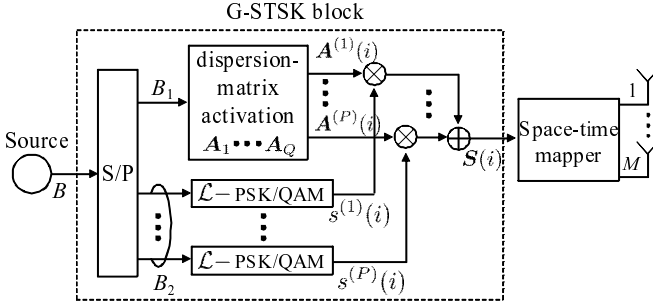
Fig. 1.  Transmitter structure of our G-STSK scheme.

TABLE I
EXAMPLE OF GSTSK$(2, 2, 2, 4, 2)$ MODULATION SCHEME OF FIG. 1, MAPPING $B = 4$ BITS PER SPACE-TIME BLOCK, WITH THE AID OF BPSK CONSTELLATION

| input bits $B = 4$ | | dispersion matrices | BPSK symbols | space-time codeword |
|---|---|---|---|---|
| $B_1=2$ | $B_2=2$ | $\boldsymbol{A}^{(1)}(i), \boldsymbol{A}^{(2)}(i)$ | $s^{(1)}(i), s^{(2)}(i)$ | $\boldsymbol{S}(i)$ |
| 00 | 00 | $\boldsymbol{A}_1, \boldsymbol{A}_2$ | $+1, +1$ | $\boldsymbol{A}_1 + \boldsymbol{A}_2$ |
| 00 | 01 | $\boldsymbol{A}_1, \boldsymbol{A}_2$ | $+1, -1$ | $\boldsymbol{A}_1 - \boldsymbol{A}_2$ |
| 00 | 10 | $\boldsymbol{A}_1, \boldsymbol{A}_2$ | $-1, +1$ | $-\boldsymbol{A}_1 + \boldsymbol{A}_2$ |
| 00 | 11 | $\boldsymbol{A}_1, \boldsymbol{A}_2$ | $-1, -1$ | $-\boldsymbol{A}_1 - \boldsymbol{A}_2$ |
| 01 | 00 | $\boldsymbol{A}_1, \boldsymbol{A}_3$ | $+1, +1$ | $\boldsymbol{A}_1 + \boldsymbol{A}_3$ |
| 01 | 01 | $\boldsymbol{A}_1, \boldsymbol{A}_3$ | $+1, -1$ | $\boldsymbol{A}_1 - \boldsymbol{A}_3$ |
| 01 | 10 | $\boldsymbol{A}_1, \boldsymbol{A}_3$ | $-1, +1$ | $-\boldsymbol{A}_1 + \boldsymbol{A}_3$ |
| 01 | 11 | $\boldsymbol{A}_1, \boldsymbol{A}_3$ | $-1, -1$ | $-\boldsymbol{A}_1 - \boldsymbol{A}_3$ |
| 10 | 00 | $\boldsymbol{A}_2, \boldsymbol{A}_4$ | $+1, +1$ | $\boldsymbol{A}_2 + \boldsymbol{A}_4$ |
| 10 | 01 | $\boldsymbol{A}_2, \boldsymbol{A}_4$ | $+1, -1$ | $\boldsymbol{A}_2 - \boldsymbol{A}_4$ |
| 10 | 10 | $\boldsymbol{A}_2, \boldsymbol{A}_4$ | $-1, +1$ | $-\boldsymbol{A}_2 + \boldsymbol{A}_4$ |
| 10 | 11 | $\boldsymbol{A}_2, \boldsymbol{A}_4$ | $-1, -1$ | $-\boldsymbol{A}_2 - \boldsymbol{A}_4$ |
| 11 | 00 | $\boldsymbol{A}_3, \boldsymbol{A}_4$ | $+1, +1$ | $\boldsymbol{A}_3 + \boldsymbol{A}_4$ |
| 11 | 01 | $\boldsymbol{A}_3, \boldsymbol{A}_4$ | $+1, -1$ | $\boldsymbol{A}_3 - \boldsymbol{A}_4$ |
| 11 | 10 | $\boldsymbol{A}_3, \boldsymbol{A}_4$ | $-1, +1$ | $-\boldsymbol{A}_3 + \boldsymbol{A}_4$ |
| 11 | 11 | $\boldsymbol{A}_3, \boldsymbol{A}_4$ | $-1, -1$ | $-\boldsymbol{A}_3 - \boldsymbol{A}_4$ |

integer $\iota$ satisfies the following inequality[1]

$$2^\iota \le \begin{pmatrix} Q \\ P \end{pmatrix} < 2^{\iota+1}. \qquad (2)$$

Firstly, $B = \log_2 f(Q, P) + P \log_2 \mathcal{L}$ input bits are S/P converted to $B_1 = \log_2 f(Q, P)$ bits and $B_2 = P \log_2 \mathcal{L}$ bits. Then, at the dispersion-matrix activation block of Fig. 1, $P$ out of $Q$ pre-assigned dispersion matrices $\boldsymbol{A}_{q'} \in \mathcal{C}^{M \times T}$ $(q' = 1, \cdots, Q)$ are activated according to $B_1 = \log_2 f(Q, P)$ input bits, in order to have $\boldsymbol{A}^{(p)}(i)$ $(p = 1, \cdots, P)$. By contrast, according to $B_2 = P \log_2 \mathcal{L}$ input bits, $P$ number of $\log_2 \mathcal{L}$ bits are separately modulated by the classic $\mathcal{L}$-point PSK/QAM modulation scheme, giving rise to the symbols $s^{(p)}(i)$ $(p = 1, \cdots, P)$. Finally, the space-time codeword $\boldsymbol{S}(i)$ is generated as follows:

$$\boldsymbol{S}(i) = \sum_{p=1}^{P} s^{(p)}(i) \boldsymbol{A}^{(p)}(i), \qquad (3)$$

where we have the power constraint of

$$\mathrm{tr}\left[\boldsymbol{A}_{q'} \boldsymbol{A}_{q'}^H\right] = \frac{T}{P} \ (q' = 1, \cdots, Q), \qquad (4)$$

in order to maintain a unity total transmission power per symbol. Here, $\mathrm{tr}[\cdot]$ represents the trace operation. We note that each of the $P$ PSK/QAM symbols $s^{(p)}(i)$ is dispersed both to the $M$ spatial and $T$ time dimensions, with the aid of the activated dispersion matrices $\boldsymbol{A}^{(p)}(i)$.

Hence, our G-STSK scheme has a set of parameters given by $M$, $N$, $T$, $Q$ and $P$. Therefore we employ the parameter-based system description of G-STSK$(M, N, T, Q, P)$ for simplicity. Additionally, the normalized throughput $R$ of our G-STSK scheme is given by

$$R = \frac{B}{T} = \frac{\log_2 f(Q, P) + P \log_2 \mathcal{L}}{T} \ \text{(bits/symbol).} \qquad (5)$$

To be more specific, in Table I we exemplify the bit-to-symbol mapping rule of QPSK-modulated ($\mathcal{L} = 2$) G-STSK$(M, N, T, 3, 2)$, where we have $f(Q, P) = 2^\iota = 2$, according to Eq. (2). As seen in Table I, the $B = 4$ input bits are S/P converted to $B_1 = 2$ bits and $B_2 = 2$ bits. According to the $B_1$ bits, $P = 2$ out of $Q = 4$ dispersion matrices are selected as $\boldsymbol{A}^{(1)}(i), \boldsymbol{A}^{(2)}(i)$, while the $B_2$ bits generate the $P = 2$ BPSK symbols $s^{(1)}(i), s^{(2)}(i)$. Finally, the space-time codeword $\boldsymbol{S}(i)$ is generated as $\boldsymbol{S}(i) = s^{(1)}(i)\boldsymbol{A}^{(1)}(i) + s^{(2)}(i)\boldsymbol{A}^{(2)}(i)$.

To elaborate a little further, according to [10], the maximum

---

[1]Although $f(Q, P)$ corresponds to $P$-out-of-$Q$ dispersion-matrix selection process and can be given by $\begin{pmatrix} Q \\ P \end{pmatrix}$ at maximum, the relationship of Eq. (2) restricts $\log_2 f(Q, P)$ to be a integer number for simplicity of the input-bit treatment.

achievable diversity order $D$ of our G-STSK scheme is given by

$$D = N \cdot \min(M, T), \qquad (6)$$

where $N$ and $\min(M, T)$ indicate the attainable receive and the transmit diversity gains, respectively. This indicates that the reduction in $T$ may give rise to the reduction of computational complexity as well as to the enhancement of the normalized throughput in Eq. (5) at the cost of a reduced diversity gain.

*B. Relationship Between Our G-STSK Scheme and Conventional MIMO Arrangements*

Next, we will demonstrate that our G-STSK scheme includes diverse MIMO arrangements.

*1) SM/SSK:* The conventional SM/SSK schemes [5]–[7] may be derived by the G-STSK$(M, N, 1, Q = M, 1)$ scheme employing the dispersion matrices of

$$\boldsymbol{A}_1 = \begin{bmatrix} 1 \\ 0 \\ \vdots \\ 0 \end{bmatrix}, \boldsymbol{A}_2 = \begin{bmatrix} 0 \\ 1 \\ \vdots \\ 0 \end{bmatrix}, \cdots, \boldsymbol{A}_Q = \begin{bmatrix} 0 \\ 0 \\ \vdots \\ 1 \end{bmatrix}, \qquad (7)$$

where the number of dispersion matrices $Q$ is set to the number of the transmit antennas $M$. As seen in Eq. (6), SM/SSK was not designed for exploiting any transmit diversity, due to the constraint of $T = 1$.

*2) LDC:* According to the system model of [10], our G-STSK framework associated with $P = Q$ has an identical system model to that of LDCs, where all of the $Q$ pre-assigned dispersion matrices are used for the linear space-time dispersion of classic PSK/QAM symbols. We note here that as implied by the relation of $B_1 = \log_2 f(Q, P) = 0$ in Eq. (2), no additional information is transmitted with the aid of the dispersion-matrix activation process in the LDC arrangement.

*3) STBC:* A class of Orthogonal STBCs (OSTBCs) is also subsumed by G-STSK upon setting $P = Q$ and using appropriately designed dispersion matrices, depending on the space-time codewords employed. For example, consider an $(M \times N) = (2 \times 2)$ QPSK-modulated Alamouti STBC [11]. Then the space-time codeword $\boldsymbol{S}(i)$

of Eq. (1) may be expressed as

$$S(i) = \frac{1}{\sqrt{2}} \begin{bmatrix} s_1 & s_2 \\ -s_2^* & s_1^* \end{bmatrix} \tag{8}$$

$$= \underbrace{\begin{bmatrix} \frac{1}{2} & 0 \\ 0 & \frac{1}{2} \end{bmatrix}}_{A_1} \sqrt{2}\alpha_1 + j \underbrace{\begin{bmatrix} \frac{1}{2} & 0 \\ 0 & -\frac{1}{2} \end{bmatrix}}_{A_2} \sqrt{2}\beta_1$$

$$+ \underbrace{\begin{bmatrix} 0 & \frac{1}{2} \\ -\frac{1}{2} & 0 \end{bmatrix}}_{A_3} \sqrt{2}\alpha_2 + j \underbrace{\begin{bmatrix} 0 & \frac{1}{2} \\ \frac{1}{2} & 0 \end{bmatrix}}_{A_4} \sqrt{2}\beta_2, \tag{9}$$

where $s_1 = \alpha_1 + j\beta_1$ and $s_2 = \alpha_2 + j\beta_2$ are two consecutive QPSK symbols per transmission block. As seen in Eq. (9), we may regard the QPSK-modulated Alamouti code as a BPSK-modulated G-STSK$(2, 2, 2, 4, 4)$ arrangement, employing $A_{q'}$ $(q' = 1, \cdots, 4)$ of Eq. (9). By following a similar decomposition process, other OSTBCs may also be represented by our G-STSK system. Moreover, it may be readily shown that other STBCs, such as Quasi-OSTBCs (QSTBCs), STBC employing Time Variant Linear Transformation (TVLT) and Threaded Algebraic STBCs (TASTBCs), are also described by our G-STSK structure, according to Section7.3 of [1].

*4) BLAST:* We may also view the BLAST architecture as a certain form of our G-STSK scheme, by setting $P = Q = M$, $T = 1$ and using Eq. (7). This BLAST arrangement does not provide any explicit transmit diversity gain, and this property is shared by the SM/SSK schemes. Since the resultant system suffers from Inter-Antenna Interference (IAI) imposed on the AEs, the computational complexity of mitigating it becomes inevitably high, which increases with the number of AEs $M$.

*5) STSK:* Furthermore, in this contribution we refer to the special case of our G-STSK scheme, employing $P = 1$, as STSK, where only one out of $Q$ dispersion matrices is activated, which results in lower $B_1$ and $B_2$ values in comparison to our G-STSK scheme for the case of $P > 1$. This STSK arrangement enables us to implement single-stream-based low-complexity ML detection, similarly to SM/SSK. Furthermore, an appropriately-constructed set of dispersion matrices $A_{q'}$ $(q' = 1, \cdots, Q)$ enables us to dispense with symbol-level IAS. More specifically, the structure of each dispersion matrix $A_{q'}$ is constructed so that there is a single non-zero element for each column of the dispersion matrix $A_{q'}$. This constraint enables us to avoid any simultaneous transmission by multiple antennas, also similarly to SM/SSK.

## III. DETECTION ALGORITHM

In this section, we present both the optimal hard-decision ML detector and the soft-detector, which are derived for our G-STSK system.

### A. Optimal Hard-Decision ML Detector

Firstly, by applying the vectorial stacking operation $vec(\ )$ to the received signal block in Eq. (1), we arrive at

$$\bar{Y}(i) = \bar{H}(i)\chi K(i) + \bar{V}(i), \tag{10}$$

where we have $\bar{Y}(i) = vec[Y(i)]$, $\bar{H}(i) = I \otimes H$, $\chi = [vec(A_1), \cdots, vec(A_Q)]$ and $\bar{V}(i) = vec[V(i)]$, while $I$ is the identity matrix and $\otimes$ is the Kronecker product. Furthermore, the $q$th element of the equivalent transmit vector $K(i)$ is assumed to be $k_q(i)$. Here, if the $q$th dispersion matrices $A_q$ is selected in the $i$th block as $A^{(p)}(i) = A_q$, $k_q(i)$ is set to the corresponding PSK/QAM symbol $s^{(p)}(i)$. Otherwise, $k_q(i)$ is zero. It should be noted that the
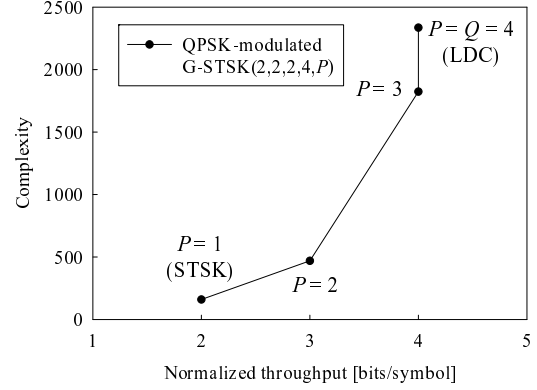


Fig. 2. The relationship between complexity and throughput of our QPSK-modulated G-STSK$(2, 2, 2, 4, P)$, achieving the maximum diversity order of four, where the parameter $P$ was changed from $P = 1$ to $P = 4$.

number of non-zero components in $K(i) = [k_1(i), \cdots, k_Q(i)]^T$ is equal to $P$.

Next, the conditional probability $P(\bar{Y}|K)$ of the linearized equivalent system model of Eq. (10) is given by

$$P(\bar{Y}|K) = \frac{1}{(\pi N_0)^{NT}} \exp\left(-\frac{\left|\left|\bar{Y} - \bar{H}\chi K\right|\right|^2}{N_0}\right). \tag{11}$$

Accordingly, the ML detection criterion is formulated as

$$(\hat{B}_1, \hat{B}_2) = \arg \max_{(B_1, B_2)} P(\bar{Y}|K) \tag{12}$$

$$= \arg \min_{(B_1, B_2)} \left|\left|\bar{Y} - \bar{H}\chi K\right|\right|^2 \tag{13}$$

$$= \arg \min_{(B_1, B_2)} \left|\left|\bar{Y} - \sum_{q=1}^{Q} k_q \left\{\bar{H}\chi\right\}_q\right|\right|^2, \tag{14}$$

where $\left\{\bar{H}\chi\right\}_q$ denotes the $q$th column of $\bar{H}\chi$. Note that the computational complexity imposed by calculating $\sum_{q=1}^{Q} k_q \left\{\bar{H}\chi\right\}_q$ in Eq. (14) linearly increases with the parameter $P$, because the number of non-zero elements in $k_q$ $(q = 1, \cdots, Q)$ is $P$ as mentioned above.

More specifically, the computational complexity per bit for the detection scheme of Eq. (14) is evaluated in terms of the number of real-valued multiplications, which may be shown to be

$$\frac{4MNT^2Q + (4NTP + 2NT)f(Q, P)\mathcal{L}^P}{B}. \tag{15}$$

Fig. 2 shows the relationship between the complexity and the throughput of our QPSK-modulated G-STSK$(2, 2, 2, 4, P)$ scheme designed for achieving the maximum diversity order of four, where the parameter $P$ was varied from $P = 1$ to $P = 4$. As mentioned in Section II, our G-STSK schemes employing $P = 1$ and $P = Q$ correspond to the STSK and LDC schemes, respectively. As seen in Fig. 2, the normalized throughput $R$ tends to increase with the value of $P$ at the cost of an increased computational complexity.

### B. Soft Demodulator

Although in Section III-A the optimal ML detector was derived for uncoded G-STSK systems, practical communication systems typically employ a powerful channel coding scheme, such as turbo coding [12]. Therefore, we hereby introduce the soft demodulator

of our G-STSK scheme, which can be used for iterative detection assisted by Soft-Input Soft-Output (SISO) decoders.

Considering that the equivalent received signal block $\bar{Y}$ in Eq. (10) conveys channel-encoded binary bits $\boldsymbol{b} = [b_1, b_2, \cdots, b_B]$, the resultant extrinsic LLR value $L_e(b_k)$ of bit $b_k$ for $k = 1, 2, \cdots, B$ may be expressed as [1] Eq. (16) as shown in the top of the next page where $K_1^k$ and $K_0^k$ represent the sub-space of the legitimate equivalent signals $\boldsymbol{K}$, which satisfy $K_1^k \equiv \{\boldsymbol{K}_{\beta_1, \beta_2} \in K : b_k = 1\}$ and $K_0^k \equiv \{\boldsymbol{K}_{\beta_1, \beta_2} \in K : b_k = 0\}$, respectively, while $\beta_1 \in \{1, \cdots, 2^{B_1}\}$ and $\beta_2 \in \{1, \cdots, 2^{B_2}\}$ are the variables corresponding to the S/P converted $B_1$ and $B_2$ input bits of Fig. 1.

Furthermore, Eq. (16) may be readily simplified by the well-known max-log approximation [12], giving rise to

$$
\begin{aligned}
L_e(b_k) = &\max_{\boldsymbol{K}_{\beta_1, \beta_2} \in K_1^k} \left[ -\frac{\left|\left|\bar{Y} - \bar{H}\chi\boldsymbol{K}\right|\right|^2}{N_0} + \sum_{j \neq k} b_j L_a(b_j) \right] \\
&- \max_{\boldsymbol{K}_{\beta_1, \beta_2} \in K_0^k} \left[ -\frac{\left|\left|\bar{Y} - \bar{H}\chi\boldsymbol{K}\right|\right|^2}{N_0} + \sum_{j \neq k} b_j L_a(b_j) \right].
\end{aligned}
\tag{17}
$$

## IV. DCMC Capacity

In this section we characterize the DCMC capacity [8] of our G-STSK framework. As mentioned above, members of the G-STSK family support many other MIMO arrangements, hence the resultant capacity equation is also applicable to diverse MIMOs.

According to [8], the DCMC capacity of our G-STSK scheme using $\mathcal{L}-$PSK/QAM signaling may be derived from that of the discrete memoryless channel as

$$
C = \frac{1}{T} \max_{P(\boldsymbol{K}_{1,1}), \cdots, P(\boldsymbol{K}_{2^{B_1}, 2^{B_2}})} \sum_{\beta_1, \beta_2} \int_{-\infty}^{\infty} \cdots \int_{-\infty}^{\infty} P(\bar{Y}|\boldsymbol{K}_{\beta_1, \beta_2})
$$
$$
\cdot P(\boldsymbol{K}_{\beta_1, \beta_2}) \log_2 \left[ \frac{P(\bar{Y}|\boldsymbol{K}_{\beta_1, \beta_2})}{\sum_{\beta_1', \beta_2'} P(\bar{Y}|\boldsymbol{K}_{\beta_1', \beta_2'}) P(\boldsymbol{K}_{\beta_1', \beta_2'})} \right] d\bar{Y}
$$
(bits/symbol). $\tag{18}$

Since Eq. (18) is maximized under the assumption that all the signals $\boldsymbol{K}_{\beta_1, \beta_2}$ are equi-probable, i.e. when we have $P(\boldsymbol{K}_{1,1}) = \cdots = P(\boldsymbol{K}_{2^{B_1}, 2^{B_2}}) = 1/2^B$, Eq. (18) is simplified to [8]

$$
\begin{aligned}
C = \frac{1}{T} \bigg( B - \frac{1}{2^B} \\
\times \sum_{\beta_1, \beta_2} E \left[ \log_2 \left\{ \sum_{\beta_1', \beta_2'} \exp(\Psi_{\beta_1, \beta_2}^{\beta_1', \beta_2'}) \bigg| \boldsymbol{K}_{\beta_1', \beta_2'} \right\} \right] \bigg),
\end{aligned}
\tag{19}
$$

where we have

$$
\Psi_{\beta_1, \beta_2}^{\beta_1', \beta_2'} = -||\bar{H}\chi(\boldsymbol{K}_{\beta_1, \beta_2} - \boldsymbol{K}_{\beta_1', \beta_2'}) + \bar{V}||^2 + ||\bar{V}||^2.
\tag{20}
$$

To be specific, in Fig. 3 we portray the DCMC capacity curves of our QPSK-modulated G-STSK$(2, 2, 2, 4, P)$ scheme, where $P$ was varied from $P = 1$ to $P = 4$. As seen in Fig. 3, upon increasing the SNR value, each capacity curve converged at its attainable normalized throughput $R$ of Eq. (5). Additionally, observe in Fig. 3 that the capacity tended to be increased with the parameter $P$, although the capacity curves corresponding to $P = 3$ and $P = 4$ were found to be almost identical.
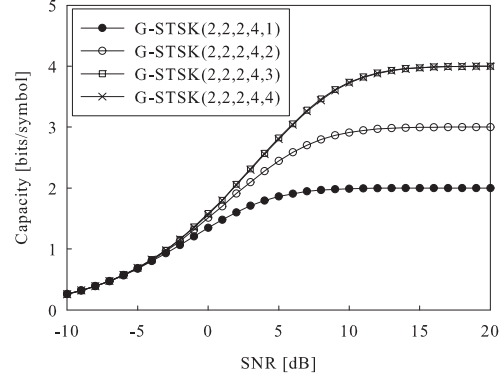


Fig. 3. DCMC capacity of the QPSK-modulated G-STSK$(2, 2, 2, 4, P)$, where $P$ was varied from $P = 1$ to $P = 4$.

## V. Performance Results

In this section the performance of our G-STSK system is characterized, while comparing the effects of diverse G-STSK parameters. In this contribution, we generated an appropriate dispersion-matrix set capable of achieving a good BER performance for each G-STSK arrangement, which were designed based on the well-known rank- and determinant-criterion [1] for the sake of simplicity, although we may readily employ other design criteria, such as the DCMC-capacity maximization technique of [1].

For the sake of saving space, we only investigated the coded G-STSK system, where we considered a serially concatenated three-stage turbo codec characterized for example in Section 7.4 of [1]. More specifically, the information bits are firstly channel-encoded by the half-rate Recursive Systematic Convolutional (RSC) code and then interleaved by the first random interleaver $\Pi_1$. Next, the interleaved bits are further encoded by the Unity-Rate Convolutional (URC) code and the URC-coded bits are then interleaved by another random interleaver $\Pi_2$. Finally, the interleaved bits are mapped to the AEs with the aid of our G-STSK mapping scheme of Fig. 1, in order to generate the space-time codewords $\boldsymbol{S}(i)$ to be transmitted to the receiver. By contrast, the receiver structure is constituted by a three-stage iterative detector, where three SISO decoders exchange their extrinsic information in the form of Log-Likelihood Ratios (LLRs). Let us assume that the RSC code is used as the *outer code*, while considering the amalgamated combination of the URC code and the G-STSK mapper to be the *inner code*.

Fig. 4 shows the EXIT curves of the QPSK-modulated G-STSK$(2, 2, 2, Q, P)$ arrangements at the SNR of 0 dB, where the parameters $(Q, P)$ were varied. We also plotted the outer RSC$(2,1,2)$ decoder's EXIT curve which employed the octal generator polynomials of $(3, 2)_8$, and the EXIT trajectory associated with the G-STSK$(2, 2, 2, 3, 2)$ scheme, where the interleaver length of both the interleavers $\Pi_1$ and $\Pi_2$ was set to 200 000 bits. This is a high interleaver length, which enables a good match between the EXIT-chart prediction and the Monte-Carlo simulation-based BER results, as detailed in [1]. Furthermore, the corresponding EXIT curves recoded for BLAST and for the Alamouti code were also shown. It can be seen in Fig. 4 that depending on the G-STSK parameters employed, the corresponding inner decoder's EXIT curve exhibited substantially different characteristics. The area within the open EXIT-tunnel determines how close the system may operate with respect to the DCMC capacity. Particularly, the inner decoder's EXIT curves of the G-STSK$(2, 2, 2, 3, 2)$ scheme exhibited the narrowest open tunnel at this SNR point, resulting in a performance which was the

$$L_e(b_k) = \frac{\sum_{\boldsymbol{K}_{\beta_1,\beta_2} \in K_1^k} P(\bar{\boldsymbol{Y}}|\boldsymbol{K}_{\beta_1,\beta_2}) \cdot \exp\left[\sum_{j \neq k} b_j L_a(b_j)\right]}{\sum_{\boldsymbol{K}_{\beta_1,\beta_2} \in K_0^k} P(\bar{\boldsymbol{Y}}|\boldsymbol{K}_{\beta_1,\beta_2}) \cdot \exp\left[\sum_{j \neq k} b_j L_a(b_j)\right]} = \frac{\sum_{\boldsymbol{K}_{\beta_1,\beta_2} \in K_1^k} \exp\left[-\frac{\left|\left|\bar{\boldsymbol{Y}} - \bar{\boldsymbol{H}}\boldsymbol{\chi}\boldsymbol{K}\right|\right|^2}{N_0} + \sum_{j \neq k} b_j L_a(b_j)\right]}{\sum_{\boldsymbol{K}_{\beta_1,\beta_2} \in K_0^k} \exp\left[-\frac{\left|\left|\bar{\boldsymbol{Y}} - \bar{\boldsymbol{H}}\boldsymbol{\chi}\boldsymbol{K}\right|\right|^2}{N_0} + \sum_{j \neq k} b_j L_a(b_j)\right]}, \quad (16)$$
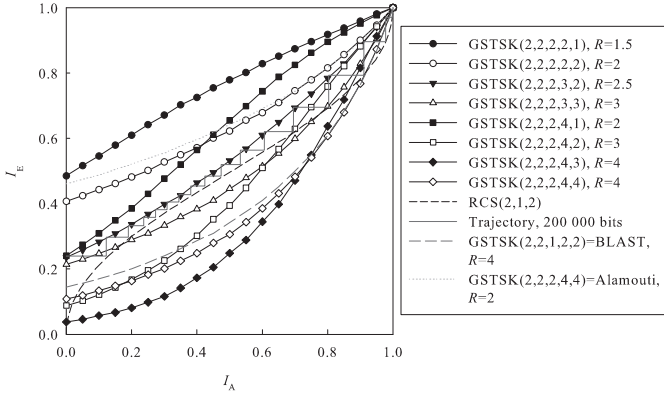


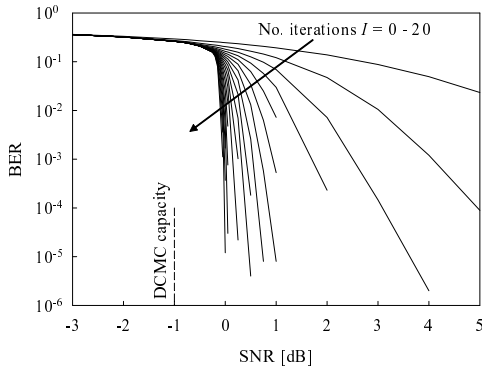Fig. 4. EXIT chart of our RSC- and URC-coded G-STSK system.



Fig. 5. Achievable BER performance of our RSC- and URC-coded G-STSK$(2,2,2,3,2)$ system employing QPSK modulation, where the number of iterations $I$ was changed from $I = 0$ to $I = 20$.

nearest to capacity for all the G-STSK arrangements. Furthermore, the Monte-Carlo simulation-based decoding trajectory demonstrated that the EXIT-chart prediction was quite accurate.

Finally, Fig. 5 shows the achievable BER performance of our RSC- and URC-coded G-STSK$(2,2,2,3,2)$ system employing QPSK modulation, achieving a total throughput of $R = 1.25$ bits/symbol. The number of iterations $I$ between the *outer* and *inner codes* was varied from $I = 0$ to $I = 20$. As predicted from the EXIT chart of Fig. 4, the corresponding BER curve exhibited an infintesimally low BER at the SNR point of 0 dB. This was within about 1 dB from the SNR corresponding to the DCMC capacity, namely from $-1.0$ dB.

In order to attain an even 'nearer-to-capacity' performance, the irregular inner- and outer-code concept [13] can be employed, where a set of EXIT curves corresponding to the diverse G-STSK parameters would allow us to create a narrower EXIT tunnel. However, it may be more practical to adaptively select one of the EXIT curves, in order to maintain an open EXIT tunnel, while increasing the achievable throughput $R$, depending on the instantaneous SNR. Additionally,

we can also introduce a threshold for controlling the computational complexity imposed by the receiver, when appropriately designing the sets of G-STSK parameters configured for near-instantaneously adaptive operation.

## VI. Conclusions

In this paper we proposed the novel G-STSK architecture, which acts as a unified MIMO framework, including many of the previously-developed MIMO arrangements, such as SM/SSK, LDC, STBC, BLAST and STSK as G-STSK's special cases. More specifically, based on the G-STSK's underlying concept, namely that $P$ out of $Q$ pre-allocated dispersion matrices are activated in conjunction with the $P$ classic PSK/QAM symbols, we can strike a flexible tradeoff between the achievable diversity order, throughput as well as computational complexity. Additionally, the unified DCMC capacity was derived for our G-STSK scheme, which also represents the capacity of other diverse MIMO arrangements.

## References

[1] L. Hanzo, O. Alamri, M. El-Hajjar, and N. Wu, *Near-Capacity Multi-Functional MIMO Systems: Sphere-Packing, Iterative Detection and Cooperation*. John Wiley and IEEE Press, 2009, **714 pages**.

[2] P. Wolniansky, G. Foschini, G. Golden, and R. Valenzuela, "V-BLAST: An architecture for realizing very high data rates over the rich-scattering wireless channel," in *Proceedings of the International Symposium on Signals, Systems, and Electronics (ISSSE'98)*, Pisa, Italy, 1998, pp. 295–300.

[3] V. Tarokh, N. Seshadri, and A. Calderbank, "Space-time codes for high data rate wireless communication: performance criterion and code construction," *IEEE Transactions on Information Theory*, vol. 44, no. 2, pp. 744–765, 1998.

[4] B. Hassibi and B. Hochwald, "High-rate codes that are linear in space and time," *IEEE Transactions on Information Theory*, vol. 48, no. 7, pp. 1804–1824, 2002.

[5] R. Mesleh, H. Haas, S. Sinanovic, C. Ahn, and S. Yun, "Spatial modulation," *IEEE Transactions on Vehicular Technology*, vol. 57, no. 4, pp. 2228–2242, 2008.

[6] J. Jeganathan, A. Ghrayeb, L. Szczecinski, and A. Ceron, "Space shift keying modulation for MIMO channels," *IEEE Transactions on Wireless Communications*, vol. 8, no. 7, pp. 3692–3703, 2009.

[7] J. Jeganathan, A. Ghrayeb, and L. Szczecinski, "Spatial modulation: optimal detection and performance analysis," *IEEE Communications Letters*, vol. 12, no. 8, pp. 545–547, 2008.

[8] S. Ng and L. Hanzo, "On the MIMO channel capacity of multidimensional signal sets," *IEEE Transactions on Vehicular Technology*, vol. 55, no. 2, pp. 528–536, 2006.

[9] S. ten Brink, "Convergence behavior of iteratively decoded parallel concatenated codes," *IEEE Transactions on Communications*, vol. 49, no. 10, pp. 1727–1737, 2001.

[10] R. Heath Jr and A. Paulraj, "Linear dispersion codes for MIMO systems based on frame theory," *IEEE Transactions on Signal Processing*, vol. 50, no. 10, pp. 2429–2441, 2002.

[11] S. Alamouti, "A simple transmit diversity technique for wireless communications," *IEEE Journal on Selected Areas in Communications*, vol. 16, no. 8, pp. 1451–1458, 1998.

[12] L. Hanzo, T. Liew, and B. Yeap, *Turbo Coding, Turbo Equalisation, and Space-Time Coding for Transmission over Fading Channels*. John Wiley and IEEE Press, 2002, **766 pages**.

[13] N. Wu and L. Hanzo, "Near-capacity irregular-convolutional-coding-aided irregular precoded linear dispersion codes," *IEEE Transactions on Vehicular Technology*, vol. 58, no. 6, pp. 2863–2871, 2009.